

# Asymmetric Transport in Long-Range Interacting Chiral Spin Chains

Javad Vahedi<sup>1,\*</sup>

<sup>1</sup>*Technische Universität Braunschweig, Institut für Mathematische Physik,  
Mendelssohnstraße 3, 38106 Braunschweig, Germany*

(Dated: August 18, 2021)

Harnessing power-law interactions ( $1/r^\alpha$ ) in a large variety of physical systems are increasing. We study the dynamics of chiral spin chains as a possible multi-directional quantum channel. This arises from the nonlinear character of the dispersion with complex quantum interference effects. Using complementary numerically and analytical techniques, we engineer models to transfer quantum states. We illustrate our approach using the long-range XXZ model modulated by Dzyaloshinskii-Moriya (DM) interaction. With exploring non-equilibrium dynamics after a local quantum quench, we identify at fully nonlocal regime (which breaks generalized Lieb-Robinson bounds) the interplay of interaction range  $\alpha$  and Dzyaloshinskii-Moriya coupling gives rise to spatially asymmetric spin excitations transport. This could be interesting for quantum information protocols to transfer quantum states and maybe testable with current trapped-ion experiments. We further explore the growth of block entanglement entropy in these systems and the order of magnitude reduction distinguished. A possible effective interaction induces by DM coupling and integrability breaking in these systems is discussed.

## I. INTRODUCTION

Recently, long-range interacting quantum systems have received an increasing attention in quantum applications[1–5]. Many natural and engineered quantum systems show long-range interactions decaying with distance  $r$  as a power law  $1/r^\alpha$ , such as van der Waals or dipole-dipole interactions. This has triggered fundamental questions related to the spreading of correlation in such systems, in particular the generalization of light-cone, picture of the Lieb-Robinson (LR) bound[6]. Comprehension the quantum dynamics in this more general case is an active field of theoretical research [7–14].

With local quenches in the long-range transverse Ising model[3, 7] and XY model[4], the behavior of correlation propagation is classified into different regimes as a function of the decay exponent  $\alpha$ . For spreading of correlation, the dynamics are divided into (i) a regime of short-range interactions where  $\alpha > 2$ , and (ii) a regime of intermediate- and long-range interactions when  $\alpha < 2$ , with certain features also changing at  $\alpha = 1$ . While the light-cone picture remains a good description for short and intermediate-range, in the case where  $\alpha < 1$ , the maximal velocity is predicted to diverge and the light-cone is no longer exists.

Noncollinear spin models with unique rotational states, such as chiral spin-spirals, have also received great attention for their application potential in spintronics and information technology and likelihood hosts for Majorana Fermions with coupled to a superconductor[15, 16]. Moreover, experiments show the importance of Dzyaloshinskii-Moriya (DM) interactions in the appearance of a spin-spiral ground state configuration[17] and the appearance and importance of a vector spin chirality,

an order parameter, in the system dynamics and transmit information down the chain[18, 19]. While linear coupling in the spin models ( $\sim \mathbf{S}_i \cdot \mathbf{S}_j$ ) favors a parallel (ferromagnetic) or antiparallel (antiferromagnetic) alignment, the DM coupling ( $\sim \mathbf{S}_i \times \mathbf{S}_j$ ) favors perpendicular alignment, which could possess a frustrated ground state[20], as well as rich three-dimensional spin skyrmion structures[21]. Moreover, long-range DM interactions showed a rich phase diagram and quantum dynamics in 1D systems[22]. The DM couplings between spins exist only when the inversion symmetry is broken at the middle point between the two spins[23, 24]. For models with inversion symmetry, the external electric field  $\vec{E}$  induces the DM interaction. Namely  $D_{ij} \sim \vec{E} \times \vec{e}_{ij}$ , where  $\vec{e}_{ij}$  is the unit vector connecting the two sites  $i$  and  $j$ .

Motivated by these possibilities, we study local quench dynamics in the long-range interacting XXZ model[3, 4] modulated with noncollinear DM interaction. While several studies on 1D systems with colinear interactions have been reported, the effect of long-range DM interactions has not been explored before (to the best of our knowledge). Using complementary numerically and analytical techniques we explore the possible quantum state engineering, and our main results on the quantum correlation spreading are summarized in Fig.1. It sketches the situation when a polarised spin state undergoes a local quench dynamics when long-range DM interaction is absent or present. It can be seen only in long-range regime case ( $\alpha < 1$ ) with modulation of DM term, quantum correlation propagates in an asymmetrically way about the perturbation. The direction in which spin excitation transport can also be controlled by DM coupling. A similar asymmetric transport has been recently reported in Abelian anyons [25]. Contrary to the Abelian anyons in which non-local anyonic commutation plays a role, in fermionic and bosonic models presented in this work complex quantum interference induces asymmetric transport.

\*Electronic address: [j.vahediaghmashhadi@tu-bs.de](mailto:j.vahediaghmashhadi@tu-bs.de)

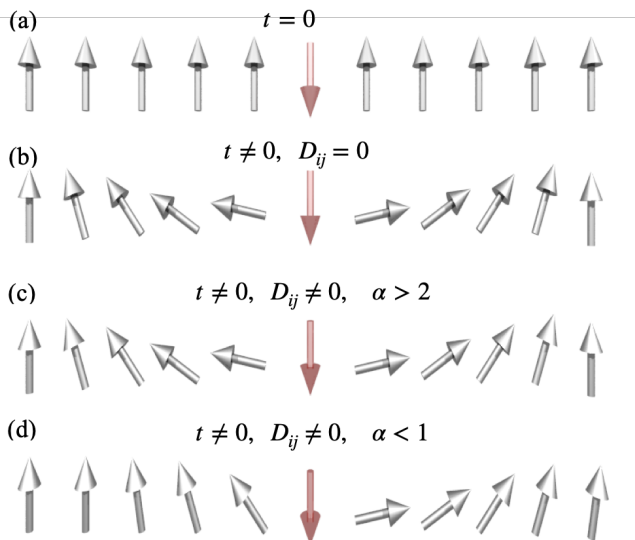


FIG. 1: (colour online) Sketch of the protocol. (a) at time  $t = 0$  initializing state with all spins aligned in the  $z$ -direction, and perturb single spin at the middle of chain by reversing its direction. Probing local spin evolution at later times (b) in the absence of DM interaction  $D_{ij} = 0$  for all range of interaction, and in the presence of DM interaction  $D_{ij} \neq 0$  at (c) short and intermediate range interaction regime  $\alpha > 2$ , (d) long-range interacting regime with  $\alpha < 1$ .

The rest of this article is arranged as follows: In Sec. II, we present the long-range models, the quantum quench protocol setup, and details of the tools we use to probe the experiment. In Sec. III, we then present the results, giving details of the methods we use to solve. We provide a summary in Sec. IV.

## II. MODELS AND OBSERVABLES

Two long-range interacting Ising[3] and XY[4] spin models have already been engineered experimentally with ion trapped technique and studied theoretically[7]. The out-of-equilibrium dynamic following local and global quenches in these two models have been investigated, and shown that at sufficiently long-range interaction, the locality is expected to be spoiled (namely, not obeying LR bound). Here, we assume it could also be feasible to engineer a long-range interaction as of DM interaction which occurs when a model is no longer symmetric under inversion[23, 24]. Having this assumption, we come up with the following long-range XXZ Hamiltonian:

$$\mathcal{H} = \sum_{i \neq j} \left[ J_{ij} (\sigma_i^x \sigma_j^x + \sigma_i^y \sigma_j^y + \Delta \sigma_i^z \sigma_j^z) + D_{ij} \cdot (\sigma_i \times \sigma_j) \right] + h \sum_i \sigma_i^z \quad (1)$$

where  $J_{ij} = J/|i-j|^\alpha$  and  $D_{ij} = D\hat{z}/|i-j|^\alpha$  with tunable exponent between infinite range ( $\alpha = 0$ ) and short-range

( $\alpha = \infty$ ),  $J$  and  $D$  denote the nearest-neighbor interaction strength,  $\Delta$  is exchange anisotropy, and  $h$  local magnetic field. In this system, the total axial magnetization  $S_{\text{total}} = \sum_{i=1}^L \sigma_i^z$  is a conserved quantity. Model is nonintegrable for all finite  $\alpha$ , but reduces to integrable models in the limit  $\alpha \rightarrow 0$ .

Local and global quenches are two well-tested protocols in the community of nonequilibrium dynamics. Here, we follow exactly the local quench setup as used in the experiment of Refs.[3, 7]. We prepare a polarised spin state in which all spins are aligned in the external field  $z$ -direction (see Fig.1-a), as a ground state of the models at extreme case  $h \gg \max\{J_{ij}, D_{ij}\}$ , then we perturb a single spin at the middle of the system by flipping its direction  $|\psi_0\rangle = \sigma_{L/2}^x |\psi_{\text{GS}}\rangle$ , as  $|\psi_0\rangle = |\uparrow \cdots \uparrow \downarrow \uparrow \cdots \uparrow\rangle$ , and observing its subsequent evolution. This can be done by probing spatially and temporally resolved spin polarization  $\langle \sigma_i^z \rangle_t$  or equal-time connected correlation function  $C_{i,L/2}(t) = \langle \sigma_i^z \sigma_{L/2}^z \rangle_t - \langle \sigma_i^z \rangle_t \langle \sigma_{L/2}^z \rangle_t$ .

The block entanglement entropy (EE) also gives interesting information of quantum correlations between two segments of a system (namely the left and right half of the chain). We will use the von Neumann entropy, which is given via

$$S_{\text{vN}}(\rho_l) \equiv S_l \equiv -\text{tr}(\rho_l \log \rho_l) \quad (2)$$

where  $\rho_l$  is reduced matrix of the left segment of chain and is defined as  $\rho_l \equiv \text{tr}_r(|\psi\rangle\langle\psi|)$ , which  $\text{tr}_r$  denotes the partial trace over the right segment of chain. In this work, we consider the EE of half of the chain  $S_{L/2}(t)$ , as its time-dependent growth summaries the buildup of quantum correlations between two halves of the chain.

Spreading information and distribution of entanglement across either side of the initial excitation in this setup could potentially be useful for application. Quantum mutual information, which gives more information on the distance of correlations[8], is the information between two distant spins  $i$  and  $j$ , and is defined via

$$\mathcal{I}_{ij} = S_{\text{vN}}(\rho_i) + S_{\text{vN}}(\rho_j) - S_{\text{vN}}(\rho_{ij}) \quad (3)$$

where  $\rho_i = \text{tr}_{k \neq i}(|\psi\rangle\langle\psi|)$  and  $\rho_j = \text{tr}_{k \neq j}(|\psi\rangle\langle\psi|)$  denote the reduced density matrices of the single spins (obtained by tracing over all other spins  $k$ ), and  $\rho_{ij} = \text{tr}_{k \neq i,j}(|\psi\rangle\langle\psi|)$  is the reduced density matrix of the composite system of the two spins.

As said before, our main goal is to explore the way correlations propagate in the model and plausible control over them. In the following section, we exploit both analytical and numerical techniques to measure the above tools to tackle the problem.

## III. RESULTS

To get an intuition, it may help to start with the nearest-neighbor (namely  $\alpha \rightarrow \infty$ ) model with  $\Delta = 0.0$  and map Hamiltonian Eq.(1) to a fermionic model.

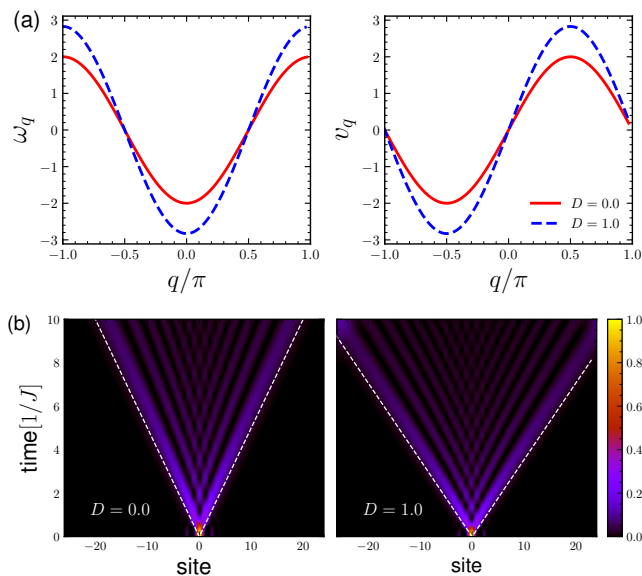


FIG. 2: (colour online) (a) Energy dispersion (left panel) relations for Hamiltonian in Eq.(4) for  $D = 0.0$  and  $D = 1.0$ . The corresponding group velocity  $v_g = \frac{d\omega_q}{dq}$  are shown in the right panel. (b) single site occupation  $\langle \psi_t | c_j^\dagger c_j | \psi_t \rangle$  versus time. Excitation at  $L/2$  spreads light-cone-like, bounded by the maximal group velocity  $v_{\max} = 2\tilde{J}$ , shown with dashed line.

This model can be solved analytically using the Jordan-Wigner transformation. For the long-range interacting case ( $\alpha$ ), the analytical fermionic picture is no longer applicable, so one can switch to the bosonic language as an analytical tool or exploit numerical techniques to inspect the dynamic of the model. To treat the many-body problem and considering the interacting term  $\Delta \neq 0.0$ , we choose the exact diagonalizing (ED) method but note that ED is limited to small system size  $L \approx 14$  due to exponential growth of the Hilbert space dimension  $2^L$ . However, to study the dynamic of many-body systems, the Krylov-space technique with exploiting the sparse structure of Hamiltonian can push limit bigger system size[26–28]. We notice for the long-range interaction the Hamiltonian matrix is not sparse as a short-range case. Nevertheless, with method we were able to reach system sizes up to  $L = 23$  with dimension  $\dim(\mathcal{H}) = 2^{23} \approx 10^7$ .

### A. Mapping to fermionic particles ( $\Delta = 0.0$ )

To understand the excitation spread, it is instructive to start with the case of nearest-interactions, i.e., with a decay exponent  $\alpha \rightarrow \infty$ , and discuss the dynamics of the quantities in this regime. In this limit, the model Hamiltonian Eq.(1) becomes a standard XX model of the form

$$\mathcal{H}_{\text{fermion}} = \sum_j \tilde{J} (\sigma_j^x \sigma_{j+1}^x + \sigma_j^y \sigma_{j+1}^y) + h \sigma_j^z \quad (4)$$

where  $\tilde{J} = \sqrt{J^2 + D^2}$ . Note that we performed a unitary transformation  $H_{\text{fermion}} = \mathcal{Q} H \mathcal{Q}^\dagger$  to eliminate the  $D$  term. Where  $\mathcal{Q} = \prod_{j \in \text{even}} e^{-i\theta \sigma_j^z}$ , and  $\tan(\theta) = -D/J$ . This model has been well studied in the literature[29–31]. Rewriting the local spin-lowering and spin-raising operators  $\sigma_j^\pm = (\sigma_j^x \pm i\sigma_j^y)/2$ , then with a Jordan-Wigner transformation, these operators can be mapped to anti-commuting quasiparticles via  $c_i = \prod_{j < i} (-1)^{\sigma_j^+ \sigma_j^-} \sigma_i^- = \prod_{j < i} (1 - 2\sigma_j^+ \sigma_j^-) \sigma_i^-$ . We thus end up with a one-dimensional noninteracting spinless fermion Hamiltonian:  $\mathcal{H}_{\text{fermion}} = \sum_j \tilde{J} (c_j^\dagger c_{j+1} + \text{h.c.}) + h c_j^\dagger c_j$ . By doing a Fourier transformation into the momentum space as  $c_j = L^{-1/2} \sum_q e^{-iqj} c_q$ , one get diagonalised Hamiltonian as  $\mathcal{H}_{\text{fermion}} = \sum_q \omega_q c_q^\dagger c_q$ , where  $\omega_q = 2(\tilde{J} \cos q + h)$ . For  $L$  spins, the quasi-momenta are given by  $q = n2\pi/L$ , where  $n = -L/2, \dots, L/2 - 1$ . The group velocity of quasiparticles is given by  $v_g = \frac{d\omega_q}{dq}$ . Fig.2-(a) shows energy dispersion relation  $\omega_q$  and the corresponding group velocity. It can be noticed that the energy is bounded with band width  $4\tilde{J}$ , and the DM interaction normalizes the coupling with a visible impact on maximum group velocity  $v_g^{\max} = 2\tilde{J}$  at  $q = \pm\pi/2$ .

Now lets explore the out-of-equilibrium dynamics. We prepare an initial state  $|\psi_0\rangle = c_{L/2}^\dagger |0\rangle$ , which in fermionic language means crating a single quasiparticle at the middle of chain as  $|0 \cdots 00100 \cdots 0\rangle_L$ . This fermionic state can be easily prepared in experiments[32]. Then we probe spreading of excitation in system with monitoring single site occupation  $\langle \psi_t | c_j^\dagger c_j | \psi_t \rangle$ , where  $|\psi_t\rangle = L^{-1/2} \sum_q e^{i(qL/2 - \omega_q t)} c_q^\dagger |0\rangle$ . With a little algebra we end up  $\langle c_j^\dagger c_j \rangle_t = L^{-2} \sum_{q_1, q_2} e^{-i(q_1 - q_2)(L/2 - j)} e^{i(\omega_{q_2} - \omega_{q_1})t}$ .

In Fig.2-(b), results for a chain with  $L = 51$  sites are illustrated. A locally perturbing system causes emitting quasiparticles at different speeds, which the fastest particles propagate at a speed  $v_g^{\max} = 2\tilde{J}$ . It gives rise to LR bound, which defines an effective causal cone for spatial correlations, outside of which the correlations are exponentially suppressed[6]. It is readily apparent that with the perturbing system at the center, excitations propagate in a symmetric way to both sides and a perfect light cone is constructed. As discussed, tuning DM interaction increases  $v_g^{\max}$ , and this is clear by comparing left ( $D = 0.0$ ) and right ( $D = 1.0$ ) panels in Fig.2-(b). For the time window present in these figures, quasiparticles for the case  $D = 1.0$  hit the boundaries. Fig.2-(a) shows that for regime  $\alpha \rightarrow \infty$ , the dispersion and corresponding velocity are bounded. This leads to a well-defined boundary of light-cone, which is clear in Fig.2-(b).

### B. Mapping to bosonic particles ( $\Delta = 0.0$ )

The presence of long-range interactions makes it impossible, as the Jordan-Wigner transformation is a non-local string operator, to map directly from the spin system to fermionic particles. However, we can use lin-

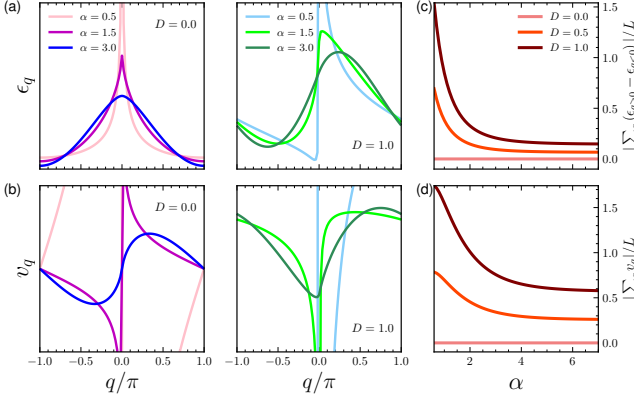


FIG. 3: (color online) (a,b) Energy dispersion  $\epsilon_q$  and corresponding group velocity  $v_q = \frac{d\epsilon_q}{dq}$  of Eq.(5) for various interactions range. Results of two DM interactions shown on left ( $D = 0.0$ ) and middle ( $D = 1.0$ ) panels, respectively. (c,d) A figure of merit which qualitatively shows asymmetric features of energy and group velocity.

ear spin-wave (LSW) theory to describe Hamiltonian in terms of quantum fluctuations around its classical ground state. For model Hamiltonian Eq.(1) with the absence of DM interaction, the validity of LSW in the presence of power-law interactions has recently been addressed[33].

We can map spin particles onto a system of hard-core bosons (magnons), introducing the Holstein-Primakoff transformation,  $\sigma_j^z \rightarrow n_j - 1/2$ ,  $\sigma_j^+ \rightarrow b_j^\dagger$ , and  $\sigma_j^- \rightarrow b_j$  where  $b_j^\dagger$  ( $b_j$ ) are the creation (annihilation) operators of hard-core bosons and  $n_i$  is the number operator at site  $i$ . These bosons obey the bosonic commutation relationships,  $[b_j, b_j^\dagger] = 1$ , with constrain  $b_j^2 = (b_j^\dagger)^2 = 0$ , such that a site either filled by one boson or empty. This can be interpreted, a spin up particle is represented by a filled site and a spin down particle by an empty site. To treat the dynamic, the picture of non-interacting magnons is only valid when  $L^{-1} \sum_q \langle b_q^\dagger b_q \rangle(t) \ll 1$  at all times, otherwise one has to account for the presence of magnons interactions.

Then we end up with a noninteracting magnonic (bosonic) Hamiltonian

$$\mathcal{H}_{\text{boson}} = \sum_{ij} \left( \mathcal{J}_{ij} b_i^\dagger b_j + \text{h.c.} \right) + h \sum_j b_j^\dagger b_j \quad (5)$$

where  $\mathcal{J}_{ij} = J_{ij} + iD_{ij}$ . The complex hopping, can be recast into a phase like term as  $\mathcal{J}_{ij} = \frac{\tilde{J} e^{i\phi}}{|i-j|^\alpha}$  with  $\phi = D/J$  independent of the decay  $\alpha$  exponent. By doing a Fourier transformation into the momentum space as  $b_j = L^{-1/2} \sum_q e^{-iqj} b_q$ , one get diagonalised Hamiltonian as  $\mathcal{H}_{\text{boson}} = \sum_q \epsilon_q b_q^\dagger b_q$ , where  $\epsilon_q = \tilde{J} \sum_{r \neq 0} \cos(qr - \phi) r^{-\alpha} + h$ . In contrast to nearest-neighbour limit, for long-range interaction on a finite system with open boundary conditions, maximal group velocity can be extracted with  $v_q^{\text{max}} \equiv$

$$|\max_q (\epsilon_{q+\pi/(L+1)} - \epsilon_q) (L+1)/\pi|.$$

Figs.3-(a,b) show the energy dispersion relation  $\epsilon_q$  and the corresponding group velocity for various interaction ranges. In the absence of DM interaction ( $D = 0.0$ , left panels of Fig.3), a clear difference going from short-range regime  $\alpha > 2$  to long-range regime  $\alpha < 1$  is visible. For regime  $\alpha > 2$ , the energy dispersion as well as its derivative are bounded i.e.  $v_q^{\text{max}} \equiv \epsilon'_q < \infty$ . As we already noted above, this ends in a clear light-cone shape of correlation spread. The situation changes for intermediate and long-range regimes  $\alpha < 2$  as a kink appear at zero momentum  $q = 0$ . While at intermediate regime  $1 < \alpha < 2$ , dispersion is bounded  $\epsilon_q < \infty$ , the velocity diverges. This enhances leakage of correlations outside of the light cone. For  $\alpha < 1$ , both dispersion and group velocity become unbounded and the light-cone disappears.

Now we turning on the DM interaction. The dispersion relation and corresponding group velocity for  $D = 1.0$  are illustrated on the middle panels of Figs.3-(a,b). As before, here also by changing interaction from short to long-range, a kink appears at  $q = 0$ . However, an asymmetry is noticeable in energy dispersion and also group velocity, which develops by complex hopping in the model. As emerges, the asymmetry is getting profound if the model exists at a long-range regime. To attain a deeper understanding, in Figs.3-(c,d), we plot a figure of merit to depict qualitatively asymmetry dependence versus decay exponent  $\alpha$ . As demonstrated, the figure of merit is zeros when  $D = 0.0$ , whereas for  $D \neq 0$  model has a certain level of asymmetry at short-range and gradually increases towards the long-range regime ( $\alpha \rightarrow 0$ ). This feature greatly impacts on correlation spreading of the model. We will show it within the quench setup introduced in the proceeding part.

We prepare an initial state with one boson at the center of the chain as  $|\psi_0\rangle = b_{L/2}^\dagger |0\rangle$ , which this bosonic state also can be prepared in experiments[34]. Fig.4 displays spatially resolved single site occupation  $\langle \psi_t | c_j^\dagger c_j | \psi_t \rangle$  versus time for  $\alpha = 1.1$ . In the absence of DM interaction, the initial excitation at the center propagates to both sides of the chain symmetrically. Although the wave-

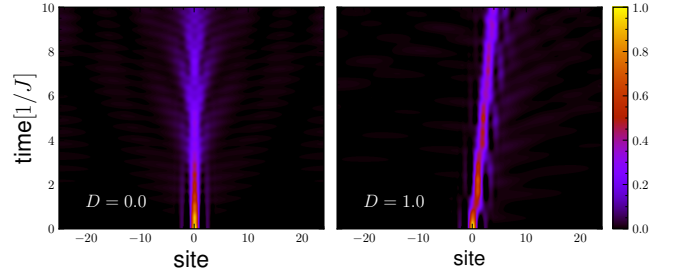


FIG. 4: (colour online) Single site bosonic particle occupation  $\langle \psi_t | b_j^\dagger b_j | \psi_t \rangle$  versus time for  $D = 0.0$  and  $D = 1.0$  depicted on left and right panels, respectively. Parameter  $\alpha = 1.1$ .



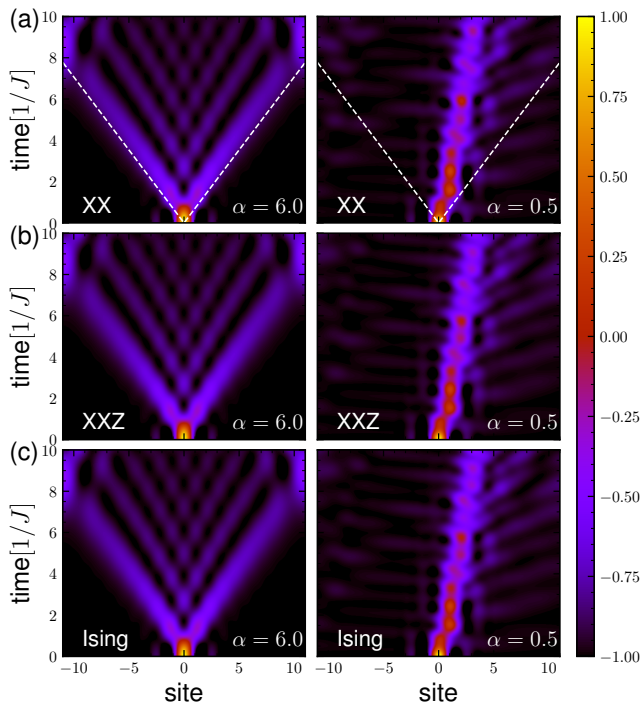


FIG. 5: (color online) Numerical exact results of spatially and temporally resolved spin polarisation  $\langle \sigma_i^z \rangle_t$  of Hamiltonian Eq.(1) (a) XX model ( $\Delta = 0.0$ ), (b) XXZ model with  $\Delta = 1.5$ , and (c) Ising model ( $\Delta \rightarrow \infty$ ) for  $D = 1.0$  at short ( $\alpha = 6.0$ ) and long ( $\alpha = 0.5$ ) interaction regimes. The dashed lines show the maximal group velocity  $v_{\max} = \tilde{J}$  of short ( $\alpha = 6.0$ ) interaction regime.

front needs finite time, the light cone is not as clear as the short interaction regime[7]. The situation changes when DM interaction is turned on. It is apparent that wavefront propagation is no longer symmetric. Indeed, if we look more closely at the right panel of Fig.4, we see that long-range DM interaction behaves as a barrier and guides the spin-wave into the desired direction[35, 36]. By changing the DM interaction, namely from  $\hat{z}$  to  $-\hat{z}$ , one can reverse propagation direction. This could be understood as follows: the phase in the hopping (in hardcore boson language) does not do anything if one has nearest-neighbor interactions, however at long-range interactions, one has closed loops, and now there are interference effects between different hopping paths where the phases come into play.

### C. Exact diagonalization

Now we tackle the problem exactly numerically as it is capable to deal with no-trivial long-range XXZ model. Using the Krylov-space technique, we probe the spin polarisation versus time. Fig.5 depicts results for Hamiltonian introduced in Eq.(1). Consistent with fermionic pictures at the nearest-neighbor limit, for local Hamil-

tonian that drives the evolution, the initially localized perturbation spread bounded by LR velocity, leading to the formation of a characteristic light cone (see top panels of Fig.5). It can be seen that the presence of DM interaction changes the propagation speed while the light-cone is still well defined (as the Hamiltonian is still local and LR bound is well defined). Increasing interaction range (decreasing  $\alpha$ ), leads to correlations spread instantaneously over the chain as shown in the right column of Fig.5. This confirms the breakdown of LR bounds similar to that of Ref.[3, 4, 7]. With the presence of long-range DM interaction, we find results consistent with the solvable spin-wave case (see top panels of Fig.5). Interestingly, with complex interference effects induced by DM coupling, spin excitation guides to the desired direction. This resembles quantum state transfer over different distances via Bloch oscillations in non-interacting chain[37].

We also address a real many-body problem, namely the long-range XXZ and Ising models, in panels (b) and (c) of Fig.5. Interestingly, except for some fine differences, the numerical results reveal these two models show the same behavior as the XX model. This calls that one could expect these behaviors to survive even in the many-body regime.

### D. Quantum information tools

It would also be interesting to have a look at the entanglement spreading in the setup. To this end, we first numerically analyze block EE.

Fig.6 displays growth of half-chain entanglement en-

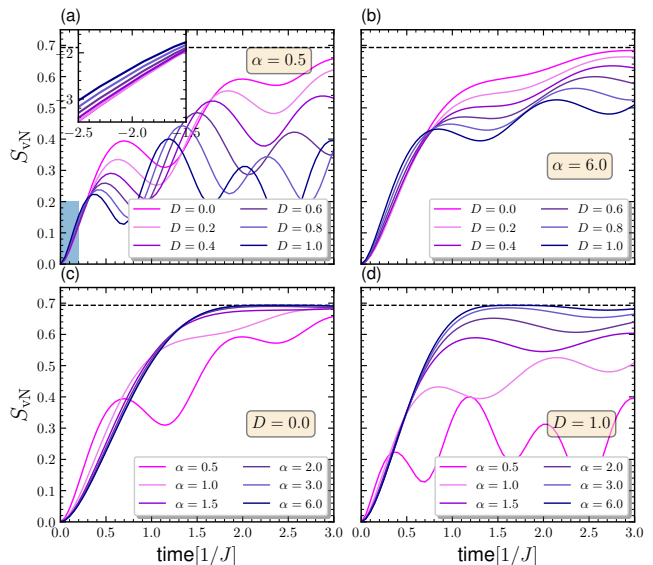


FIG. 6: (colour online) Growth of half-chain entanglement entropy  $S_{vN}$  for various parameters in the Hamiltonian of Eq.(1). The horizontal dashed line is saturate value  $S_{vN}(t) = \log 2$ . Insert plot illustrates shaded area in logarithmic scale. Data for chain size  $L = 23$  and  $\Delta = 0.5$ .

trophy  $S_{\text{vN}}$ . In all sets of parameters shown here,  $S_{\text{vN}}(t)$  initially grows as a power of time  $t$  and at longer time saturates to  $S_{\text{vN}}(t) = \log 2$  independent of system regime. Figs.6(a,b) present results for long-range ( $\alpha = 0.5$ ) and short-range ( $\alpha = 6.0$ ) regimes with different DM coupling strength. By increasing DM, the linear (in logarithmic scale) behavior of  $S_{\text{vN}}$  breaks down and changes into an oscillatory before entering the saturation regime. As observed, while the presence of DM coupling modulates a higher value of entanglement at a smaller time, it finds lower entanglement at later times (where boundary effects become important). This situation is more profound in the long-range regime as correspondingly the boundary effects shift to earlier times. Figs.6(c,d) illustrate results for a fixed DM coupling with increasing power exponent  $\alpha$ . In the absence of DM coupling (Fig.6-(c)) and for intermediate and short-range regimes (i.e.  $\alpha > 1.0$ ), the half-chain entropy initially increases as a power of  $t$ . Remarkably, the presence of DM interaction has a great impact on entanglement growth at short-range regime (i.e.  $\alpha < 1.0$ ). In Fig.6(d), one can see with changing  $\alpha$ ,  $S_{\text{vN}}$  faces a few orders of reduction. This may show a signature of diffusive rather than ballistic transport in the chain. Although a detailed study in this line needs separate work, we give some elaboration on this issue in the appendix.

At the experimental level, this is more straightforward to measure quantum mutual information than the von Neumann entropy. So further confirmation may be accessed by inspection quantum mutual information between two distant spins  $\mathcal{I}_{ij}$ . In Fig.7, we have plotted a figure of merit to measure quantum information polarization

$$\Delta\mathcal{I} = \left| \frac{\mathcal{I}_{1,L/2} - \mathcal{I}_{L,L/2}}{\mathcal{I}_{1,L/2} + \mathcal{I}_{L,L/2}} \right|$$

between spin located at centre with spins are sitting at edges of chain. For comparison purposes, results for three different regimes are presented in the same time window. Noticeably, we find that, for intermediate and long-range regimes (i.e.  $\alpha \lesssim 2.0$ ) distant spins become entangled instantaneously, whereas short-range regime quasiparticle peaks need a certain time reach edges (consistent with LR bound). Furthermore, we notice that, in the absence of DM term, no matter what is the range of interaction,  $\Delta\mathcal{I}$  is always zero which confirms the symmetric spread of quantum information to either side of the chain. In contrast for  $\alpha < 2$ , the presence of DM term changes the way quantum information spreads over the chain. Interestingly, as shown in Fig.7, by gradually tuning the DM coupling strength quantum information  $\Delta\mathcal{I}$  increases and even may reach a fully polarized one for some time intervals.

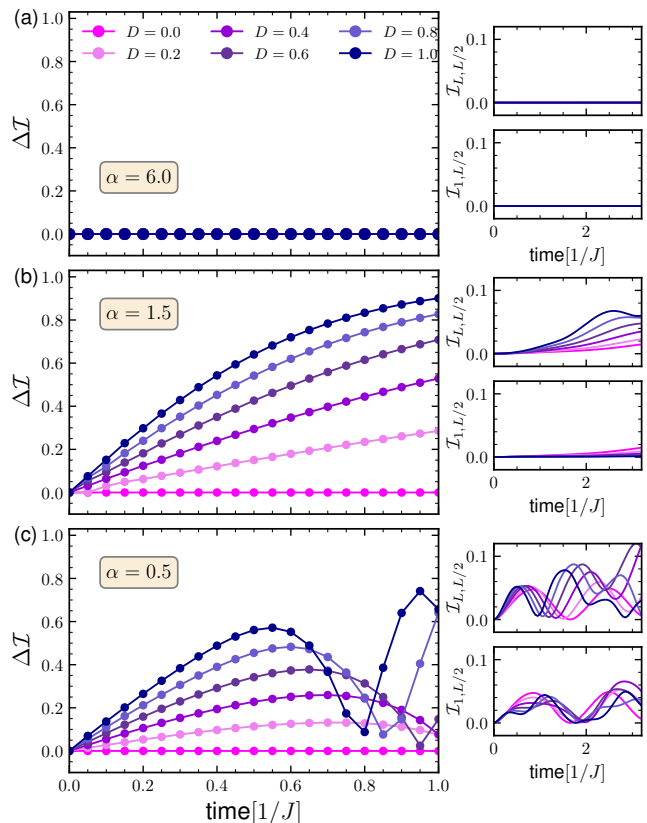


FIG. 7: (colour online) Main panels (a-c) show time evolution of quantum mutual information polarization  $\Delta\mathcal{I}$  between spin at centre (place of initial perturbation) and the spins located at edges of chain. Side panels correspond to the quantum mutual information  $\mathcal{I}_{ij}$  of the main panel. Data for chain size  $L = 23$  and  $\Delta = 0.5$ .

#### IV. SUMMARY AND OUTLOOK

Recently, long-range spin chains have gained attention as platforms to study quantum information dynamics. The possibility of controlling the power-law interactions and vector chirality of DM coupling in a variety of materials and systems put forward an idea that one can use that to drive information along the chain. We proposed a protocol setup consisting long-range spin-1/2 chain modulated with DM coupling. For translationally invariant fermionic or bosonic models, information spreading occurs in a spatially symmetric way. However, our results reveal transport spin excitation in the desired path by inter-playing interaction range and DM coupling direction. This may have technical consequences for our ability to design quantum information protocols as a unidirectional and bidirectional quantum channel and maybe testable with current state-of-the-art trapped-ion experiments. We further explore the growth of block entanglement entropy in these systems and the order of magnitude reduction distinguished. A possible effective interaction induces by DM coupling and integrability break-

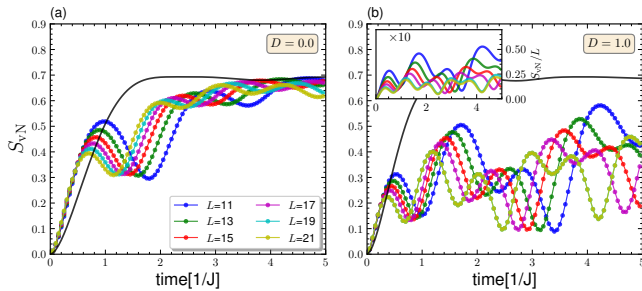


FIG. 8: (colour online) Growth of half-chain entanglement entropy  $S_{vN}$  of Hamiltonian Eq.(1) with  $\Delta = 0.5$  for various different chain length at long-range regime with  $\alpha = 0.5$ . Where DM interaction (a)  $D = 0.0$ , (b)  $D = 1.0$ . The solid-black line is data for nearest-neighbour case ( $\alpha \rightarrow \infty$ ). Inset shows  $S_{vN}$  scaled with chain length.

ing in these systems is discussed. This issue could also be interesting to simulate the quantum system on a computer, which typically linear growth of entanglement during time evolution, making numerical simulations often unfeasible[38–40]. Finally, it would be interesting to study the effects of long-range DM interactions on other systems, e.g. many-body localized systems [41, 42], or long-range disorder spin chains[43].

## V. ACKNOWLEDGEMENT

I would like to express my gratitude to Prof. Christoph Karrasch for their financial support of my stay in his group. Thanks to Y. Mohdeb for his reading of the manuscript. The ED calculations have been performed at the Centre De Calcul (CDC), CY Cergy Paris Université.

### Appendix: Half-chain entanglement growth

In this appendix, we aim to have more analysis on  $S_{vN}$ . Fig.8 plots results of entanglement growth for different system sizes. Interestingly, the results at the long-range regime show clear size dependence with reduction of entanglement growth at thermodynamic limit. The effect of DM interaction is also visible with comparing panels (a) and (b). Although, at the long-range regime and for short times,  $S_{vN}$  increases faster than the nearest-neighbor case (see the solid-black line in Fig.8), but a suppression at a later time is profound.

### Appendix: Chaotic feature

The presence of DM interaction breaks the time reversal symmetry, so the model belongs to the Gaussian unitary ensemble (GUE) universality class. To get

more insight, we utilize two well-stabilized tools from the quantum chaos community, the level spacing statistics (LSS)[44] and the inverse participation ratios (IPRs)[45]. While the former refers to the correlation among the energy spectrum, the latter is a measure of localization-delocalization of a given state of a quantum mechanical system concerning a preferential basis. To avoid any possible level crossing due to symmetries, we have found the full spectrum of Hamiltonian in subspace  $S_{total}^z = 1.0$  with open boundary conditions. Results for various parameters are displayed in Figs.9-10, for chain length  $L = 17$ .

At short-range limit (see the red histogram in Figs.9-10 (a) and (b)), probability distribution  $P(s)$  displays Poissonian LSS, as is typical for integrable. It could be easily understood as the extreme nearest-neighbor case which can be trivially integrated into momentum space for Ising and XX models or solved with Bethe ansatz for XXZ model[46]. While at long-range regime with the presence of DM coupling, model systematically develops level repulsion, as is typical for non-integrable models (see the blue histogram in Figs.9 (b)). This is also well captured by the narrow spreading of IPR on the computational basis (here  $\sigma_z$ ) with comparing Figs.9-10 (c) and (d).

This also implies that long-range DM interaction can break integrability and act as a form of effective interaction. Therefore a systematic study in a separate work on conductivity in this model could serve as a future direction.

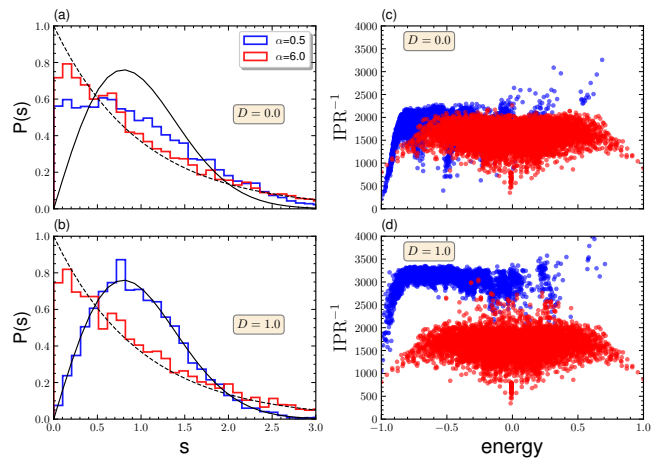


FIG. 9: (colour online) Level spacing distribution of Hamiltonian Eq.(1) at short- and long-range for DM interaction (a)  $D = 0.0$  and (b)  $D = 1.0$ . Dashed and solid black lines give the theoretical curves  $P_{\text{Poisson}}(s) = \exp(-s)$  and Wigner-Dyson surmise  $P_{\text{WD}}(s) = (\pi s/2) \exp(-\pi s^2/4)$ . Panels (c) and (d) are their corresponding IPRs. Chain length is  $L = 17$ ,  $\Delta = 0.0$  and we work on subspace  $S_{total}^z = 1.0$  as the Hamiltonians introduced in Eq.(1) commutes with  $[\mathcal{H}, S_{total}^z] = 0$ .

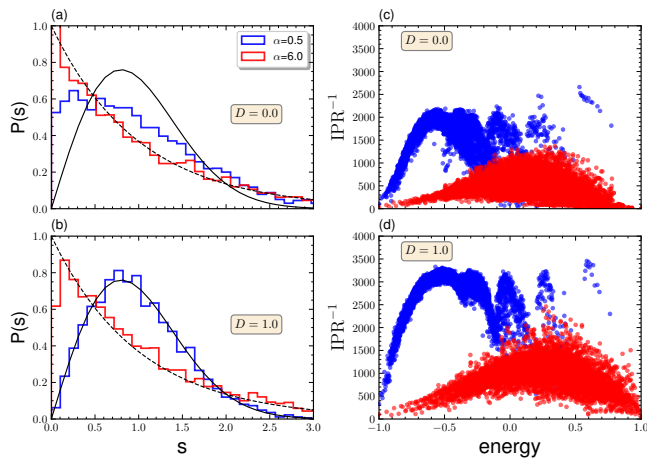


FIG. 10: (colour online) Same as figure 9, but for  $\Delta = 1.5$

- [1] P. Schauß, M. Cheneau, M. Endres, T. Fukuhara, S. Hild, A. Omran, T. Pohl, C. Gross, S. Kuhr, and I. Bloch, *Nature* **491**, 87 (2012), URL <https://doi.org/10.1038/nature11596>.
- [2] R. Islam, C. Senko, W. C. Campbell, S. Korenblit, J. Smith, A. Lee, E. E. Edwards, C.-C. J. Wang, J. K. Freericks, and C. Monroe, *Science* **340**, 583 (2013), ISSN 0036-8075, URL <https://science.sciencemag.org/content/340/6132/583>.
- [3] P. Jurcevic, B. P. Lanyon, P. Hauke, C. Hempel, P. Zoller, R. Blatt, and C. F. Roos, *Nature* **511**, 202 (2014), URL <https://doi.org/10.1038/nature13461>.
- [4] P. Richerme, Z.-X. Gong, A. Lee, C. Senko, J. Smith, M. Foss-Feig, S. Michalakis, A. V. Gorshkov, and C. Monroe, *Nature* **511**, 198 (2014), URL <https://doi.org/10.1038/nature13450>.
- [5] C.-L. Hung, A. González-Tudela, J. I. Cirac, and H. J. Kimble, *Proceedings of the National Academy of Sciences* **113**, E4946 (2016), ISSN 0027-8424, URL <https://www.pnas.org/content/113/34/E4946>.
- [6] E. H. Lieb and D. W. Robinson, *Communications in Mathematical Physics* **28**, 251 (1972), URL <https://doi.org/10.1007/BF01645779>.
- [7] P. Hauke and L. Tagliacozzo, *Phys. Rev. Lett.* **111**, 207202 (2013), URL <https://link.aps.org/doi/10.1103/PhysRevLett.111.207202>.
- [8] J. Schachenmayer, B. P. Lanyon, C. F. Roos, and A. J. Daley, *Phys. Rev. X* **3**, 031015 (2013), URL <https://link.aps.org/doi/10.1103/PhysRevX.3.031015>.
- [9] A. S. Buyskikh, M. Fagotti, J. Schachenmayer, F. Essler, and A. J. Daley, *Phys. Rev. A* **93**, 053620 (2016), URL <https://link.aps.org/doi/10.1103/PhysRevA.93.053620>.
- [10] J. Zeiher, J.-y. Choi, A. Rubio-Abadal, T. Pohl, R. van Bijnen, I. Bloch, and C. Gross, *Phys. Rev. X* **7**, 041063 (2017), URL <https://link.aps.org/doi/10.1103/PhysRevX.7.041063>.
- [11] I. Frérot, P. Naldesi, and T. Roscilde, *Phys. Rev. Lett.* **120**, 050401 (2018), URL <https://link.aps.org/doi/10.1103/PhysRevLett.120.050401>.
- [12] F. Liu, R. Lundgren, P. Titum, G. Pagano, J. Zhang, C. Monroe, and A. V. Gorshkov, *Phys. Rev. Lett.* **122**, 150601 (2019), URL <https://link.aps.org/doi/10.1103/PhysRevLett.122.150601>.
- [13] A. Leroose, B. Žunkovič, A. Silva, and A. Gambassi, *Phys. Rev. B* **99**, 121112 (2019), URL <https://link.aps.org/doi/10.1103/PhysRevB.99.121112>.
- [14] M. K. Joshi, A. Elben, B. Vermersch, T. Brydges, C. Maier, P. Zoller, R. Blatt, and C. F. Roos, *Phys. Rev. Lett.* **124**, 240505 (2020), URL <https://link.aps.org/doi/10.1103/PhysRevLett.124.240505>.
- [15] S. Nadj-Perge, I. K. Drozdov, J. Li, H. Chen, S. Jeon, J. Seo, A. H. MacDonald, B. A. Bernevig, and A. Yazdani, *Science* **346**, 602 (2014), ISSN 0036-8075, URL <https://science.sciencemag.org/content/346/6209/602>.
- [16] S. Jeon, Y. Xie, J. Li, Z. Wang, B. A. Bernevig, and A. Yazdani, *Science* **358**, 772 (2017), ISSN 0036-8075, URL <https://science.sciencemag.org/content/358/6364/772>.
- [17] M. Steinbrecher, R. Rausch, K. T. That, J. Hermenau, A. A. Khajetoorians, M. Potthoff, R. Wiesendanger, and J. Wiebe, *Nature Communications* (2018), URL <https://doi.org/10.1038/s41467-018-05364-5>.
- [18] H. Katsura, N. Nagaosa, and A. V. Balatsky, *Phys. Rev. Lett.* **95**, 057205 (2005), URL <https://link.aps.org/doi/10.1103/PhysRevLett.95.057205>.
- [19] M. Menzel, Y. Mokrousov, R. Wieser, J. E. Bickel, E. Vedmedenko, S. Blügel, S. Heinze, K. von Bergmann, A. Kubetzka, and R. Wiesendanger, *Phys. Rev. Lett.* **108**, 197204 (2012), URL <https://link.aps.org/doi/10.1103/PhysRevLett.108.197204>.
- [20] J. Vahedi and S. Mahdaviifar, *The European Physical Journal B* **85**, 171 (2012), URL <https://doi.org/10.1140/epjb/e2012-20784-0>.
- [21] A. Fert, N. Reyren, and V. Cros, *Nature Reviews Materials* **2**, 17031 (2017), URL <https://doi.org/10.1038/natrevmats.2017.31>.
- [22] E. Vernek, O. Ávalos-Ovando, and S. E. Ulloa, *Phys. Rev. B* **102**, 174427 (2020), URL <https://link.aps.org/doi/10.1103/PhysRevB.102.174427>.



- [org/doi/10.1103/PhysRevB.102.174427](https://doi.org/10.1103/PhysRevB.102.174427).
- [23] I. Dzyaloshinsky, *Journal of Physics and Chemistry of Solids* **4**, 241 (1958), ISSN 0022-3697, URL <https://www.sciencedirect.com/science/article/pii/S0022369758900763>.
- [24] T. Moriya, *Phys. Rev.* **120**, 91 (1960), URL <https://link.aps.org/doi/10.1103/PhysRev.120.91>.
- [25] F. Liu, J. R. Garrison, D.-L. Deng, Z.-X. Gong, and A. V. Gorshkov, *Phys. Rev. Lett.* **121**, 250404 (2018), URL <https://link.aps.org/doi/10.1103/PhysRevLett.121.250404>.
- [26] A. Nauts and R. E. Wyatt, *Phys. Rev. Lett.* **51**, 2238 (1983), URL <https://link.aps.org/doi/10.1103/PhysRevLett.51.2238>.
- [27] Y. Saad, *SIAM Journal on Numerical Analysis* **29**, 209 (1992), URL <https://doi.org/10.1137/0729014>.
- [28] M. Brenes, V. K. Varma, A. Scardicchio, and I. Girotto, *Computer Physics Communications* **235**, 477 (2019), ISSN 0010-4655, URL <http://www.sciencedirect.com/science/article/pii/S0010465518303060>.
- [29] S. Mahdavifar, Z. Bakhshipour, J. Vahedi, and M. R. Soltani, *Journal of Superconductivity and Novel Magnetism* **28**, 1807 (2015), URL <https://doi.org/10.1007/s10948-014-2944-y>.
- [30] J. Vahedi, A. Ashouri, and S. Mahdavifar, *Chaos: An Interdisciplinary Journal of Nonlinear Science* **26**, 103106 (2016), URL <https://doi.org/10.1063/1.4964745>.
- [31] F. Mofidnakhai, F. K. Fumani, S. Mahdavifar, and J. Vahedi, *Phase Transitions* **91**, 1256 (2018), URL <https://doi.org/10.1080/01411594.2018.1527916>.
- [32] U. Schneider, L. Hackermüller, J. P. Ronzheimer, S. Will, S. Braun, T. Best, I. Bloch, E. Demler, S. Mandt, D. Rasch, et al., *Nature Physics* **8**, 213 (2012), URL <https://doi.org/10.1038/nphys2205>.
- [33] I. Frérot, P. Naldesi, and T. Roscilde, *Phys. Rev. B* **95**, 245111 (2017), URL <https://link.aps.org/doi/10.1103/PhysRevB.95.245111>.
- [34] J. P. Ronzheimer, M. Schreiber, S. Braun, S. S. Hodgman, S. Langer, I. P. McCulloch, F. Heidrich-Meisner, I. Bloch, and U. Schneider, *Phys. Rev. Lett.* **110**, 205301 (2013), URL <https://link.aps.org/doi/10.1103/PhysRevLett.110.205301>.
- [35] T. Ramos, B. Vermersch, P. Hauke, H. Pichler, and P. Zoller, *Phys. Rev. A* **93**, 062104 (2016), URL <https://link.aps.org/doi/10.1103/PhysRevA.93.062104>.
- [36] B. Vermersch, T. Ramos, P. Hauke, and P. Zoller, *Phys. Rev. A* **93**, 063830 (2016), URL <https://link.aps.org/doi/10.1103/PhysRevA.93.063830>.
- [37] D. Tamascelli, S. Olivares, S. Rossotti, R. Osellame, and M. G. A. Paris, *Scientific Reports* **6**, 26054 (2016), URL <https://doi.org/10.1038/srep26054>.
- [38] U. Schollwöck, *Annals of Physics* **326**, 96 (2011), ISSN 0003-4916, January 2011 Special Issue, URL <https://www.sciencedirect.com/science/article/pii/S0003491610001752>.
- [39] M. Schwarz, K. Temme, and F. Verstraete, *Phys. Rev. Lett.* **108**, 110502 (2012), URL <https://link.aps.org/doi/10.1103/PhysRevLett.108.110502>.
- [40] G. Evenbly and G. Vidal, *Phys. Rev. Lett.* **112**, 240502 (2014), URL <https://link.aps.org/doi/10.1103/PhysRevLett.112.240502>.
- [41] M. Schreiber, S. S. Hodgman, P. Bordia, H. P. Lüschen, M. H. Fischer, R. Vosk, E. Altman, U. Schneider, and I. Bloch, *Science* **349**, 842 (2015), ISSN 0036-8075, URL <https://science.sciencemag.org/content/349/6250/842>.
- [42] D. A. Abanin, E. Altman, I. Bloch, and M. Serbyn, *Rev. Mod. Phys.* **91**, 021001 (2019), URL <https://link.aps.org/doi/10.1103/RevModPhys.91.021001>.
- [43] Y. Mohdeeb, J. Vahedi, N. Moure, A. Roshani, H.-Y. Lee, R. N. Bhatt, S. Kettemann, and S. Haas, *Phys. Rev. B* **102**, 214201 (2020), URL <https://link.aps.org/doi/10.1103/PhysRevB.102.214201>.
- [44] A. Ashouri, S. Mahdavifar, G. Misguich, and J. Vahedi, *Annalen der Physik* **532**, 1900515 (2020), URL <https://onlinelibrary.wiley.com/doi/abs/10.1002/andp.201900515>.
- [45] S. Moshfegh, A. Ashouri, S. Mahdavifar, and J. Vahedi, *Physica A: Statistical Mechanics and its Applications* **516**, 502 (2019), ISSN 0378-4371, URL <https://www.sciencedirect.com/science/article/pii/S0378437118313943>.
- [46] H. Bethe, *Zeitschrift für Physik* **71**, 205 (1931), ISSN 0044-3328, URL <https://doi.org/10.1007/BF01341708>.